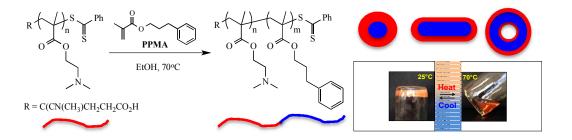# RAFT Dispersion Polymerisation of 3-Phenylpropyl Methacrylate with Poly[2-(dimethylamino)ethyl methacrylate] Macro-CTAs in Ethanol and Associated Thermoreversible Polymorphism

R = C(CN(CH₃)CH₂CH₂CO₂H)

Journal Name

ARTICLE

RAFT Dispersion Polymerization of 3-Phenylpropyl Methacrylate with Poly[2-(dimethylamino)ethyl methacrylate] Macro-CTAs in Ethanol and Associated Thermoreversible Polymorphism

Yiwen Pei, Nadia C. Dharsana, Johannes A. van Hensbergen, Robert P. Burford, Peter J. Roth and Andrew B. Lowe*

The direct synthesis of methacrylic-based soft polymeric nanoparticles via reversible addition-fragmentation chain transfer dispersion polymerization (RAFTDP) is described. The use of poly[2-(dimethylamino)ethyl methacrylate]s, of varying average degree of polymerization ($\bar{X}_n$), as the stabilizing blocks for the RAFTDP of 3-phenylpropyl methacrylate (PPMA) in ethanol at 70°C, at various total solids contents, yielded the full spectrum of self-assembled nanoparticles (spherical and worm aggregates and polymersomes). We also demonstrate that nanoparticle morphology can be tuned simply by controlling temperature. This is especially evident in the case of worm aggregates undergoing a thermoreversible transition to spherical species – a process that is accompanied by a macroscopic degelation-gelation process.

Introduction

The ability of block copolymers, especially AB diblock copolymers, to undergo self-directed assembly in a selective solvent for one block to give polymeric nanoparticles exhibiting rich polymorphism is well documented.[1-6] Historically this has been achieved via the synthesis of well-defined block copolymers (most commonly via living anionic polymerization) with predetermined molecular weights and compositions under homogeneous conditions followed by molecular self-association in a selective solvent. Inducing assembly can be achieved by direct dissolution in a selective solvent (this is only recommended for certain copolymer compositions) or by initial molecular dissolution in a non-selective solvent followed by dilution with a selective solvent (this is commonly followed by dialysis against the selective solvent to remove the non-selective species). With the discovery and development of the range of reversible deactivation radical polymerization processes it is now possible to prepare a huge number of novel functional block copolymers giving access to a likewise impressively large array of self-assembled soft nanoparticles.

Of the 'common' soft matter nano-aggregates, i.e. spheres, worm/cylindrical species and vesicles (aka polymersomes), spherical aggregates are by far the most prevalent reported and studied species in the literature. The adopted morphology of an aggregated block copolymer is determined by many factors

with the free energy (force) balance between the stretching of the polymer chains in the aggregate core, excluded volume (chain repulsion) effects associated with the coronal polymer chains and the interfacial surface energy at the core/corona boundary being important considerations.[7-9] As such, nanoparticle morphology may be controlled by varying the relative ratio of the solvophilic and solvophobic chains, i.e. copolymer composition, or by tuning the interfacial surface energy for a fixed copolymer composition and concentration. Importantly, in the context of the work presented herein, nanoparticle morphology may also be controlled by solvent-induced changes in the core dimensions and the volume fraction of solvent present in the core. This was nicely demonstrated by Yu and Eisenberg in amphiphilic block copolymers of polystyrene (PS) and poly(acrylic acid) (PAA)[9] and proposed by Nagarajan.[10] It is also possible to employ environmental triggers, e.g. temperature, to induce (reversible) morphological changes in the self-assembled state although examples of such systems are comparatively rare. For example, Abbas et al.[11] described the step-wise change in morphology from spheres to worms to vesicles (S-W-V) in dilute solutions of poly(styrene-b-dimethylsiloxane) copolymers by employing mixtures of dialkyl phthalates to tune selectivity. The reverse V-W-S transitions were observed simply by heating and were demonstrated to be totally reversible. Similarly, LaRue and co-workers[12] reported thermally-induced morphology transitions in

poly(styrene-*b*-isoprene) copolymers (for a fixed composition and concentration) in heptane between 25 and 40°C, in which the solvent quality changed for both blocks upon heating. Room temperature worm aggregates rearranged to spherical species upon heating and likewise, vesicles transformed to worms. The transitions were reversible although the S-W transition required more than 36 days at 25°C to achieve appreciable rearrangement to the worm phase.

Recently there has been growing interest in so-called polymerization-induced self-assembly (PISA), *i.e.* the *in situ* formation of polymeric nanoparticles, of varying morphology, during polymerization. In recent years this has best been exemplified by descriptions of reversible addition-fragmentation chain transfer dispersion polymerization (RAFTDP). A key feature of RAFTDP is that it allows for the straightforward preparation of a range of soft matter nanoparticles (spherical/worm aggregates, polymeric vesicles and compound vesicles for example) simply by controlling the relative ratio of the solvophilic stabilizing block and the solvophobic comonomer block or the relative solids content during block copolymer syntheses. Indeed, the general utility of RAFTDP for preparing such self-assembled species directly *in situ* has been demonstrated by a number of research groups with various combinations of stabilizing macro-CTAs, comonomers and polymerization media including nonpolar solvents, water, alcohols and supercritical CO_2.[13-30]

While RAFTDP represents a more straightforward approach for the synthesis of self-assembled polymeric nanoparticles it is not as versatile as the more traditional post-polymerization processing approach since the number of comonomers that can be employed in RAFTDP formulations is significantly more limited (fewer substrates exhibit the required monomer solubility/polymer insolubility characteristics in a given solvent). For example, the majority of the current literature focuses on styrene,[25, 27-29, 31] and a number of methacrylic species[15, 19, 20, 32-36] as the core-forming comonomers. There are also several examples of thermally responsive comonomer building blocks such as *N*-isopropylacrylamide (NIPAM)[23, 37] and *N,N*-diethylacrylamide (DEA)[38] in certain aqueous systems where the well-established inverse temperature dependent solubility of polyNIPAM and polyDEA is exploited to induce phase separation and self-assembly as the polymerizations proceed. Also, it is worth highlighting that some of the reported systems appear to be best suited to formulations in which the conversion of the solvophobic comonomer block, particularly styrene, is limited to low-to-intermediate values, which is not ideal from a scale-up or commercialisation perspective. However, all-methacrylic systems can, and commonly are, taken to high conversions of the comonomer. Given the limited reported monomer pool exploited in RAFTDP, we recently began an evaluation of alternative, less common, substrates as potential comonomers in such formulations. Our initial focus has been on certain aryl methacrylates. For example, we recently detailed the first examples of the RAFTDP of 2-phenylethyl methacrylate (PEMA) with poly[2-(dimethylamino)ethyl methacrylate] (PDMAEMA) macro-

CTAs in ethanol.[39] We demonstrated that PEMA is a suitable comonomer for RAFTDP and could be easily employed in the preparation of spherical and worm-like micelles as well as higher ordered vesicular species. Additionally, we also noted that the tertiary amine residues in the stabilizing PDMAEMA coronal chains could be reacted with 1,3-propanesultone yielding the first examples of the analogous zwitterionic (betaine) self-assembled species.

Building on this report, herein we detail our recent studies regarding the RAFTDP of 3-phenylpropyl methacrylate (PPMA) employing PDMAEMA macro-CTAs in alcoholic media, Scheme 1. We demonstrate that PPMA is a suitable comonomer for RAFTDP and under appropriate conditions yields AB diblock copolymers that self-assemble *in situ* giving nanoparticles exhibiting the full spectrum of self-assembled morphologies. We also highlight an interesting thermoreversible degelation-gelation process associated with worm micelles that is accompanied by a solvent induced W-S morphology transition.

Experimental

All reagents were purchased from the Aldrich Chemical Company and used as received unless noted otherwise. 2,2'-Azobis(isobutyronitrile) (AIBN) was purified by recrystallization twice from methanol. 2-(Dimethylamino)ethyl methacrylate (DMAEMA) and 3-phenylpropyl methacrylate (PPMA) were passed through a basic Al_2O_3 column to remove inhibitor prior to use. 4-Cyanopentanoic acid dithiobenzoate (CPADB) was prepared according to a procedure described elsewhere.[40]

Synthesis of poly[2-(dimethylamino)ethyl methacrylate] macro-CTAs

A general procedure for the RAFT homopolymerization of DMAEMA mediated by CPADB is as follows:

A solution containing 2-(dimethylamino)ethyl methacrylate (10.0 g, 0.06 mol), CPADB (0.3 g, 1.06 mmol), AIBN (27.0 mg, 0.17 mmol) in acetonitrile (10.0 mL) was added to a reaction vessel equipped with a magnetic stir bar. The reaction vessel was sealed with a rubber septum and the solution purged with nitrogen for 15 min prior to being immersed in a preheated oil bath set at 70°C. The DMAEMA homopolymer(s) were isolated by precipitation into *n*-hexane followed by Buchner filtration. Samples were dried at 40°C *in vacuo* overnight.

Typical RAFT dispersion polymerization procedure

Below is given a typical RAFTDP procedure employing PDMAEMA$_{20}$ and PPMA as the comonomer at a total solids content of 21 wt%. The same general procedure was employed for all other RAFTDP syntheses.

To a reaction vial was added 3-phenylpropyl methacrylate (0.2 g, 0.979 mmol), AIBN (0.46 mg, 0.003 mmol), PDMAEMA$_{20}$ macro-CTA (58.0 mg, 0.014 mmol), triethylamine (10 mol%

excess based on PDMAEMA residues) and ethanol (0.95 g). The reaction vessel sealed and purged with nitrogen prior to immersion in a preheated oil bath set at 70°C. Polymerisation was allowed to proceed for 24 h. The final monomer conversion was determined by ^{1}H NMR analysis by integrating the PPPMA peak (C_6H_5-) at δ = 7.10-7.50 ppm to the PPMA monomer vinyl peak (CH_2) at δ = 5.5 and 6.1 ppm.

Copolymer Characterization

NMR spectroscopic measurements were performed on a Bruker Avance III 500 instrument equipped with a 31P-TBI probe operating at 500.13 MHz for hydrogen nuclei. Experiments were run with a 7500 Hz sweep width, 3.2 s acquisition time and 2 s recycle delay. The pulse program employing solvent suppression at two ^{1}H chemical shifts was employed to eliminate residual water signals and the ethyl resonance associated with d_6-EtOH. The internal solvent signal of $CDCl_3$ was used as reference (δ ($CHCl_3$) = 7.26 ppm), and all chemical shifts are reported in ppm (δ). For the temperature-dependent NMR studies samples were heated to the target temperature and held at that temperature for at least 10 min prior to data acquisition.

The number average molecular weight, $\overline{M}_{n,NMR}$, and the average degree of polymerization, $\overline{X}_n$, were estimated based on the integral values of the signals at δ = 4.06 ppm and 7.30 –

7.90 ppm, as shown in Equation 1.

$$\overline{X}_n(PDMAEMA) = 5 \times I(4.06\ ppm)/2 \times I(7.30\text{-}7.90\ ppm) \quad (1)$$

where I(4.06 ppm) and I(7.30-7.90 ppm) are the integral values assigned to one of the methylene groups on the PDMAEMA side chains (the $-CH_2$ adjacent to the ester group) and aryl protons of the phenyl dithioester end-groups respectively.

Size exclusion chromatography (SEC) was performed on a Shimadzu system with four phenogel columns (10^2, 10^3, 10^4, 10^6 Å pore size) in tetrahydrofuran (THF) operating at a flow rate of 1 mL min^{-1} at 40°C using a RID-10A refractive index detector. Chromatograms were analyzed by Cirrus SEC software version 3.0. The system was calibrated with a series of narrow molecular weight distribution polystyrene standards with molecular weights ranging from 0.58-1820 kg mol^{-1}.

Transmission electron microscopy (TEM) imaging was conducted at 100 kV on a JEOL1400 TEM. To prepare TEM samples, 5.0 μL of a dilute copolymer solution (0.7 w/w%) was deposited onto a copper grid (ProSciTech), stained with uranyl acetate (0.2 w/w% in water) and dried under ambient conditions. For TEM grid preparation at high temperature all materials and equipment were placed in a hot oven at the desired temperature for at least 10 min. The 21wt% PDMAEMA-b-PPPMA copolymer samples were kept under

Table 1 Summary of the block copolymer compositions, monomer conversion, molecular weight determined by ^{1}H NMR spectroscopy and end group analysis, the dispersity ($Đ_M = \overline{M}_w/\overline{M}_n$) and number-average molecular weight ($\overline{M}_n$) as determined by SEC, the DLS-measured hydrodynamic diameters (D_h) and polydispersities (μ_2/Γ^2) and the observed TEM morphology, for the RAFTDP of 3-phenylpropyl methacrylate with PDMAEMA$_{20}$ and PDMAEMA$_{35}$ macro-CTAs in ethanol at 70°C. All polymerisations were conducted at 21 wt% solids.

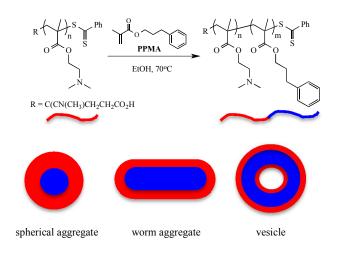| Entry number, block copolymer – and their NMR measured composition	[M]/ [Macro-CTA]	NMR		SEC $\overline{M}_n$ and $Đ_M$	DLS		TEM morphology
		PPMA % conv.	$\overline{M}_{n,NMR}$		D_h (nm)	μ_2/Γ^2	
(1) PDMAEMA$_{20}$-b-PPPMA$_{24}$	25	96	8,300	9,000 / 1.22	12.8	0.15	spheres
(2) PDMAEMA$_{20}$-b-PPPMA$_{34}$	35	97	10,400	11,500 / 1.22	21.7	0.03	spheres
(3) PDMAEMA$_{20}$-b-PPPMA$_{42}$	43	97	12,000	11,900 / 1.19	23.9	0.17	spheres + worms
(4) PDMAEMA$_{20}$-b-PPPMA$_{47}$	50	94	13,000	12,500 / 1.19	21.9	0.22	worms
(5) PDMAEMA$_{20}$-b-PPPMA$_{53}$	55	97	14,200	14,100 / 1.20	230.9	0.82	worms + vesicles
(6) PDMAEMA$_{20}$-b-PPPMA$_{56}$	60	94	14,800	14,700 / 1.13	98.8	1.00	worms + vesicles
(7) PDMAEMA$_{20}$-b-PPPMA$_{61}$	65	94	15,900	14,900 / 1.12	132.4	0.38	vesicles
(8) PDMAEMA$_{20}$-b-PPPMA$_{71}$	75	94	17,900	15,800 / 1.23	492	0.42	vesicles
(9) PDMAEMA$_{20}$-b-PPPMA$_{92}$	100	92	22,200	19,200 / 1.22	705	0.89	vesicles
(10) PDMAEMA$_{35}$-b-PPPMA$_{63}$	65	97	18,600	15,700 / 1.23	38.2	0.20	spheres
(11) PDMAEMA$_{35}$-b-PPPMA$_{80}$	85	95	22,100	19,600 / 1.23	51.2	0.33	spheres + worms
(12) PDMAEMA$_{35}$-b-PPPMA$_{92}$	95	97	24,600	21,600 / 1.23	57.5	0.27	spheres + worms
(13) PDMAEMA$_{35}$-b-PPPMA$_{108}$	115	94	27,800	25,600 / 1.24	70.6	0.27	spheres + worms
(14) PDMAEMA$_{35}$-b-PPPMA$_{127}$	135	94	31,700	37,200 / 1.23	134.1	0.27	worms + vesicles

continuous stirring at a desired temperature for 5 min and then diluted to 0.70 wt% with heated ethanol (at the same temperature as the copolymer sample) prior to TEM sample preparation. The TEM grids were then stained as detailed above.

Dynamic light scattering (DLS) measurements were performed using a Malvern Instrument Zetasizer Nano Series instrument equipped with a 4 mW He-Ne laser operating at 633 nm and an avalanche photodiode (APD) detector. The scattered light was detected at an angle of 173°. For sample preparation, 0.1 mL of the parent RAFTDP solution was diluted with 2.9 mL of ethanol and the solution then sonicated for 5 min prior to double filtration through 0.45 μm nylon filters.

The glass transition temperature of poly(3-phenylpropyl methacrylate) was determined by dynamic scanning calorimetry (DSC) on a TA instruments DSC-2010 differential scanning calorimeter. 16 mg of sample was weighed into an aluminium pan that was sealed with a crimped lid. The sample, and reference, pans were cooled to ~ -100°C with liquid nitrogen and heated under a blanket of nitrogen at a rate of 5°C min^{-1} to a final temperature of 200°C. Relative heat flow through the sample was recorded as a function of temperature.

Results and discussion

Scheme 1 RAFTDP of 3-phenylpropyl methacrylate with poly[2-(dimethylamino)ethyl methacrylate] macro-CTAs in ethanol at 70°C.

In this study two poly[2-(dimethylamino)ethyl methacrylate] (PDMAEMA) homopolymers were employed as macro-CTAs in the ethanolic RAFTDP of 3-phenylpropyl methacrylate (PPMA), Scheme 1. To the best of our knowledge, this is the first time PPMA has been employed as a comonomer in RAFTDP. The PDMAEMA homopolymers were synthesised via homogeneous RAFT polymerization under standard conditions employing CPADB as the mediating agent and AIBN as the source of primary radicals.[39] We targeted PDMAEMA homopolymers with low average degrees of polymerization ($\bar{X}_n$) since we,[39] and others,[15, 19] have noted that stabilising macro-CTAs with low $\bar{X}_n$'s give the best chance of capturing the full range of self-assembled nanoparticle morphologies in subsequent RAFTDPs (above a critical $\bar{X}_n$ of the solvophilic block the ability to access higher ordered morphologies becomes increasingly more difficult). PDMAEMA homopolymers with ^{1}H NMR-determined $\bar{X}_n$'s of 20 ($\bar{M}_{n,NMR}$ = 3,140; $\bar{M}_{n,SEC}$ = 2,600; $Đ_M$ = 1.16) and 35 ($\bar{M}_{n,NMR}$ = 5,750; $\bar{M}_{n,SEC}$ = 8,900; $Đ_M$ = 1.11), were obtained and employed as macro-CTAs in subsequent block copolymerizations.

RAFTDP of PPMA and the effect of solvophobic block length at a fixed total solids content

To examine the suitability of PPMA as a comonomer in RAFTDP we initially examined the block copolymerization of PPMA employing the PDMAEMA$_{20}$ macro-CTA at a concentration of 21 wt% total solids. Table 1 gives a summary of the PDMAEMA$_{20}$-b-PPPMA$_y$ copolymers prepared, their conversions and compositions, ^{1}H NMR-determined molecular weights, SEC-measured dispersities ($Đ_M$) and number average molecular weights ($\bar{M}_n$), DLS measured hydrodynamic diameters (D_h) and polydispersities (μ_2/Γ^2) and the TEM-observed nanoparticle morphology. The series of block copolymers were prepared with target $\bar{X}_n$'s of the PPMA block spanning the range 25-100. In all instances, copolymerization proceeded smoothly with high to near-quantitative conversions of PPMA being observed. The absolute molecular weights, as determined by ^{1}H NMR spectroscopy, increased with increasing length of the PPMA block, as expected, while SEC analysis confirmed successful block copolymer formation with the measured $Đ_M$'s ≤ 1.23, Table 1 and Figure 1. Blocking efficiency is high, as evidenced by the lack of detectable macro-CTA, however, in all instances we observe some higher molecular weight termination products derived from polymer radical coupling reactions that, technically, can be considered impurities. However, one of the advantages of RAFTDP is that since such species are generally only formed at high, to very high, monomer conversion they have little, if any, effect on the resulting nanoparticle morphology, which is the primary structural feature of concern in these studies.

Each of the PDMAEMA$_{20}$-b-PPPMA$_y$ copolymers was also characterized by TEM, Table 1. In this particular series, at 21 wt% solids, we observed the full sphere-to-worm-to-vesicle (S-W-V) transitions (including intermediate mixed phases) with increasing $\bar{X}_n$ of the PPMA block. Figure 2 shows representative TEM images for the nanoparticles obtained for entries 2-7 in Table 1.
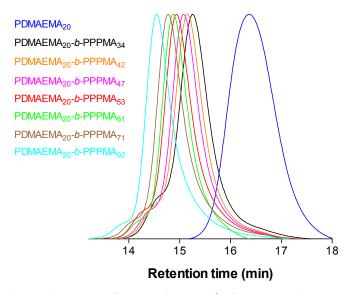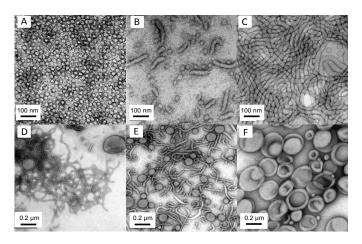
Figure 1 The experimentally measured SEC traces for the PDMAEMA$_{20}$-b-PPPMA$_y$ series of block copolymers prepared by RAFTDP in EtOH at 70°C. Their associated dispersities and SEC/NMR determined molecular weights are given in Table 1.

Figure 2 Representative TEM images of the nanoparticles formed from PDMAEMA$_{20}$-b-PPPMAy diblock copolymers prepared at a total solids concentration of 21 wt% in EtOH at 70°C with y = (A) 34, (B) 42, (C) 47, (D) 53, (E) 56, and (F) 61 (entries 2-7 Table 1).

In the case of the PDMAEMA$_{20}$-b-PPPMA$_{24}$ and PDMAEMA$_{20}$-b-PPPMA$_{34}$ copolymers, both formed nanoparticles with an observed spherical morphology (Figure 2A shows a TEM image for the PPPMA$_{34}$-based block copolymer). The observed TEM size of ca. 15-20 nm for this block copolymer agrees well with the hydrodynamic diameter (D_h) measured by DLS (21.7 nm, μ_2/Γ^{-2} = 0.03, Table 1, entry 2). Increasing $\overline{X}_n$ further to a species with 42 PPMA repeat units, Table 1 entry 3, gives a product that exhibits a mixed morphology with the nanoparticles consisting of spheres and short 'oligomeric' worms formed by the coalescence of a small number of the spherical aggregates, Figure 2B. Mixed phases are a common feature of RAFTDP at, or near, key compositions associated with morphology transitions, and are a reflection of the molecular weight and compositional distributions associated

with the block copolymers. A further, small, increase in the $\overline{X}_n$ of the PPMA block to 47 yields a species that forms a pure worm nanoparticle phase, Figure 2C, in which the length of the worms is now on the order of hundreds of nanometres. The diameter of the worms, as estimated by TEM, is comparable to the D_h of the precursor spheres and is not unexpected. However, the D_h value for the worms, as measured by DLS, should be treated with caution (even though it appears to be reasonable) since the Stokes-Einstein equation is only valid for hard spheres and thus D_h values for worms are strictly 'sphere equivalent' values. In the case of the PDMAEMA$_{20}$-b-PPPMA$_{53}$ and PDMAEMA$_{20}$-b-PPPMA$_{56}$ copolymers, Table 1 entries 5 and 6 and Figure 1D and 1E, further mixed morphologies consisting of worms and vesicles are observed with an apparent larger proportion of vesicles in the case of the latter block copolymer. The PDMAEMA$_{20}$-b-PPPMA$_{61}$ copolymer, Table 1 entry 7 and Figure 2F, gives nanoparticles with a pure vesicular morphology albeit with a rather broad size distribution. DLS indicates an average D_h of ca. 132 nm (μ_2/Γ^{-2} = 0.38) that is not unreasonable given the representative TEM image that clearly shows the presence of spherical species around this average size. For the two most asymmetric block copolymers, PDMAEMA$_{20}$-b-PPPMA$_{71}$ and PDMAEMA$_{20}$-b-PPPMA$_{92}$, final two entries in Table 1, larger vesicles are observed with DLS measured sizes of ca. 500 and 700 nm respectively.

In the case of the PDMAEMA$_{35}$ macro-CTA with PPMA at 21 wt% solids we observe the same general trend, $i.e.$ a systematic change in morphology from spheres to worms to vesicles, with an increasing length of the solvophobic PPMA block. The systematic S-W-V transitions observed for these series of DMAEMA-PPMA AB diblock copolymers are consistent with the effect of an increasing $\overline{X}_n$ of the solvophobic block for a fixed $\overline{X}_n$ of solvophilic block. Interestingly, for similar ratios of DMAEMA:PPMA, morphological differences are observed between the PDMAEMA$_{20}$ and PDMAEMA$_{35}$ series of block copolymers. For example, while a pure worm nanoaggregate phase is observed for the PDMAEMA$_{20}$-b-PPMA$_{47}$ copolymer (block ratio of 0.43), the PDMAEMA$_{35}$ based copolymer with an identical PPPMA block ratio (0.43) gives a mixed phase consisting of spheres and worms. Indeed, this mixed S + W phase for the PDMAEMA$_{35}$ block copolymers is observed up to a block ratio of at least 0.32 while the PDMAEMA$_{20}$-b-PPPMA$_{61}$ copolymer (block ratio of 0.33) gives a pure vesicular morphology. These results reinforce the advantage of employing a stabilising block of relatively low $\overline{X}_n$ in terms of more ready accessibility to a desired morphological self-assembled state.

Table 2 Summary of the block copolymer compositions, monomer conversion, molecular weight determined by ^{1}H NMR spectroscopy and end group analysis, the dispersity ($Đ_M = \overline{M}_w/\overline{M}_n$) and number-average molecular weight ($\overline{M}_n$) as determined by SEC, the DLS-measured hydrodynamic diameters (D_h) and polydispersities (μ_2/Γ^2) and the observed TEM morphology, for the RAFTDP of 3-phenylpropyl methacrylate with PDMAEMA$_{35}$ macro-CTAs in ethanol at 70°C at variable total solids contents.

Entry number, block copolymer – and their NMR measured composition	[M]/ [Macro-CTA]/ solids content	NMR		SEC $\overline{M}_n$ and $Đ_M$	DLS		TEM morphology
		PPMA % conv.	$\overline{M}_{n,NMR}$		D_h (nm)	μ_2/Γ^2	
(1) PDMAEMA$_{35}$-*b*-PPPMA$_{76}$	85 / 10 wt%	90	21,300	17,900 / 1.24	49.3	0.16	spheres
(2) PDMAEMA$_{35}$-*b*-PPPMA$_{80}$	85 / 21 wt%	95	22,100	19,600 / 1.23	51.2	0.33	spheres + worms
(3) PDMAEMA$_{35}$-*b*-PPPMA$_{82}$	85 / 30 wt%	97	22,500	20,500 / 1.24	63.3	0.36	spheres + worms
(4) PDMAEMA$_{35}$-*b*-PPPMA$_{83}$	85 / 40 wt%	98	22,700	21,500 / 1.24	123.1	0.32	worms

Effect of total solids concentration for a fixed DMAEMA-PPMA block copolymer composition.

The effect of total solids concentration, for a fixed block copolymer composition, is also known to have an effect on the adopted self-assembled morphology.[15, 39] Employing the PDMAEMA$_{35}$ macro-CTA we examined a series of RAFTDPs at variable total solids spanning the range of 10-40 wt% for a target $\overline{X}_n$ of PPMA of 85 at 100% conversion. The results are summarized in Table 2 and representative TEM images are shown in Figure 3.
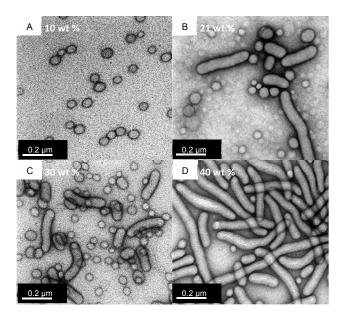

Figure 3 Representative TEM images for the DMAEMA-PPMA block copolymers of identical molar composition prepared at variable total solids concentration: (A) 10wt%, (B) 21wt%, (C) 30 wt% and (D) 40wt%.

The DMAEMA-PPMA block copolymers were successfully prepared with near quantitative conversion of PPMA to give well-defined copolymers with reasonably narrow molecular weight distributions ($Đ_M$'s ≤ 1.24), with little evidence of high molecular weight termination products and NMR-determined absolute molecular weights that are uniform.

At 10 wt% a pure spherical morphological is observed with a DLS-measured D_h of 49.3 nm and a corresponding polydispersity of 0.16. The 21 and 30 wt% formulations both yield nanoparticles exhibiting mixed phases consisting of spheres and worms. However, the worms are generally very short and are more 'cigar-like' suggesting these particular formulations give systems that exist at the early stages of spherical aggregate fusion, *i.e.* at the S-W transitional boundary. The worm nanoparticles have a TEM determined diameter that is similar to that of the spheres, and as expected, is consistent with the assumption that worm formation occurs via the direct 1D coalescence of spherical particles. The 40 wt% sample gives an essentially pure worm phase with uniform diameters and lengths that are on the order of hundreds of nanometres. These results further highlight the importance of concentration as an experimental parameter than can be utilized as a means of controlling nanoparticle morphology in RAFTDP systems.
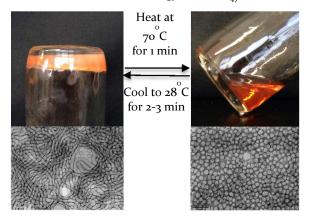
Worm aggregates and thermoreversible degelation-gelation

In the case of the DMAEMA$_{20}$-*b*-PPMA$_{47}$ block copolymer prepared at 21 wt% solids a 100% worm phase was observed at ambient temperature (Table 1 entry 4). Interestingly, macroscopic thermoreversible degelation-gelation behaviour was observed for this particular block copolymer. The formation of a room temperature physical gel by polymeric worm aggregates (as a result of worm entanglements above some critical concentration, c^*) is not unexpected, certainly at the concentration under which they were prepared, and has been reported previously in the case of small molecule surfactants that have the ability to form worm-like nanoaggregates.[41, 42] Additionally, Armes and co-workers have reported several examples of thermoreversible degelation-gelation in block copolymer worm systems prepared by RAFTDP in *aqueous* media.[32, 43-45] However, with one exception, their observed reported behaviour was opposite to that described below with their systems generally transforming from a gelled to a free flowing state upon *cooling*.

During the preparation of the PDMAEMA$_{20}$-*b*-PPPMA$_{47}$ block copolymer at 21 wt% we noticed that at the polymerization temperature of 70°C the solution was

essentially transparent and fluid while after cooling to RT the sample became gelled. TEM analysis of the RT sample indicated a pure worm phase morphology as detailed above, Figure 4. Interestingly, the physical gel only required heating at 70°C for 1 min to become a free flowing solution. This macroscopic transition from a gel to a fully fluid state could be due to one of three possible reasons: (i) complete disentanglement of the worm nanoparticles; (ii) a fundamental morphology change, or (iii) molecular dissolution of the block copolymer chains at the higher temperature. A sample of the free flowing solution was extracted at 70°C, diluted with hot EtOH and rapidly dried on a TEM grid. Visualization demonstrated that the thermally promoted degelation process is accompanied by a fundamental W-S morphology transition, Figure 4. Since spheres cannot form physical entanglements this morphology switch is the fundamental mechanism for the observed degelation phenomenon. Similar W-S morphological transitions were shown to be the cause of the observed reversible gelation reported by Armes *et al.*[43, 45]

PDMAEMA$_{20}$-*b*-PPPMA$_{47}$

Figure 4 Digital pictures of a 21wt% solution, in EtOH, of the PDMAEMA$_{20}$-*b*-PPPMA$_{47}$ copolymer at room temperature highlighting the gel-like state and worm aggregate morphology, and the same sample after heating to 70°C in a fluid state with the aggregates now exhibiting a spherical morphology. This behaviour is completely reversible.

As noted, this behaviour is completely reversible. Cooling the free flowing solution back to just above RT results in reformation of the gel state within only 2-3 min. These observations highlight an important consideration when characterizing self-assembled soft matter nanoparticles prepared by RAFTDP. Specifically, the morphology formed and observed (especially when sampled at elevated temperature) may not coincide with the room temperature morphological state, *i.e.* different morphologies associated with the *same* block copolymer may be observed under rather narrow thermal conditions. Fortuitously, this is visually apparent in the case of worm nanoparticle systems due to the

associated degelation-gelation phenomena observed at the typically high RAFTDP concentrations, but may not be macroscopically obvious with other thermally promoted morphological transitions.

The ability of the PDMAEMA$_{20}$-*b*-PPPMA$_{47}$ block copolymer to undergo such rapid morphological transitions suggests these soft matter nanoparticles are highly dynamic over the temperature range examined. The rearrangement, or exchange, of block copolymer chains in the assembled state is generally slow compared to small molecule surfactants, and the factors affecting exchange kinetics can be complicated.[46, 47] For example, many polymeric nanoparticles are considered kinetically frozen, *i.e.* there is no chain exchange between aggregates and unimers or other aggregate species, and it is not uncommon to observe self-assembled species even after dilution below the critical aggregation concentration or for morphological transitions to require days, weeks or months to be complete, *vide supra*.[12] One important property when considering the chain dynamics and ability of polymeric nanoaggregates to rearrange is the glass transition temperature (T_g) of the core-forming block. While, technically, a solid-state property we note that in general core blocks with high T_g's, *e.g.* polystyrene (T_g varies with MW but is commonly *ca.* 100°C[48]) or poly(methyl methacrylate) (T_g can vary from *ca.* 20 to > 120°C depending on MW and tacticity[49]), give self-assembled species that can be kinetically frozen with the cores being considered 'glassy',[50, 51] while core-forming blocks with sub-ambient T_g's can allow for facile rearrangement. However, a low T_g alone does not guarantee favourable exchange/rearrangement dynamics and, for example, a high interfacial surface energy or large hydrophobic block length can still result in kinetically locked aggregates.[52] Additionally, the relative degree of core solvation is an important factor since this determines, in part, the extent of mobility of the core polymer chains. This prompted us to measure the T_g of PPPMA and to evaluate the relative core solvation over the temperature range observed for the reversible W-S transition. We prepared a low molecular weight PPPMA homopolymer by conventional RAFT polymerization ($\bar{M}_{n,SEC}$ = 16,600; $Đ_M$ = 1.09) and measured its T_g via differential scanning calorimetry (DSC). DSC analysis indicated a T_g of 2°C implying that even in a completely desolvated state in a nanoparticle core the PPPMA block is amorphous. We note that this measured value is significantly lower than the literature values for structurally related poly(2-phenylethyl methacrylate) (T_g = 42°C)[53, 54] and poly(benzyl methacrylate) (T_g = 54°C),[55] both of which have been utilized as comonomers in alcoholic RAFTDP formulations. This sub-ambient T_g for the PPPMA core-forming block suggests that the occurrence of temperature-induced morphological transitions in DMAEMA-PPMA AB diblock copolymers at elevated temperature will not be restricted by the physical nature of the PPPMA core block.

^{1}H NMR spectroscopy was employed to qualitatively evaluate the temperature effect on the solvent quality for either, or both, blocks. Figure 5 shows a series of ^{1}H NMR spectra, recorded in d_6-EtOH, spanning the temperature range 25-75°C for the PDMAEMA$_{20}$-*b*-PPPMA$_{47}$ copolymer. There are several pertinent features in Figure 5. While we see an increase in key resonances associated with the coronal PDMAEMA block (d and b) indicating enhanced solubility with increasing temperature, the key features are those labelled a and c associated with the core-forming PPPMA block.
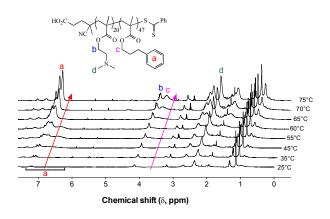

Figure 5 A waterfall plot of ^{1}H NMR spectra of the PDMAEMA$_{20}$-*b*-PPPMA$_{47}$ copolymer recorded in d_6-EtOH spanning the temperature range 25-75°C

There is a clear increase in the intensity of these signals (more evident in the case of the aromatic hydrogens labelled a) indicating an increasing degree of solvation with increasing temperature. The major onset of enhanced solvation of the side chain aromatic groups appears to occur at *ca*. 55°C with increasing solvation of the functional groups closer to the backbone (*e.g.* c) beginning to occur at the higher temperature of *ca*. 65°C. While a simple inspection of the ^{1}H NMR spectra at 70 or 75°C might lead to the conclusion that the block copolymer is molecularly dissolved at these highest temperatures, a closer inspection of the integrals associated with the core-forming PPMA blocks with those of the stabilising PDMAEMA chain indicate that the PPMA blocks do not become fully solvated and we can confidently state that these are not molecularly dissolved at these high temperatures. Also, recall that TEM analysis indicates that the PDMAEMA$_{20}$-*b*-PPPMA$_{47}$ copolymer exists as spherical aggregates at 70°C. Figure 6A shows the ^{1}H NMR spectrum of the PDMAEMA$_{20}$-*b*-PPPMA$_{47}$ copolymer at 75°C while inset is a plot of the relative integrals of the aromatic (red) and O-CH$_2$ (pink) hydrogens normalized to an integral associated with PDMAEMA. This plot indicates that the PPMA aromatic hydrogens become essentially fully solvated at *ca*. 45°C, or rather, the ratio of the integral of these aromatic species with those of PDMAEMA do not change at temperatures exceeding this value. In contrast, the relative integral associated with the PPMA OCH$_2$ group reaches a maximum value of *ca*. 0.65 of its
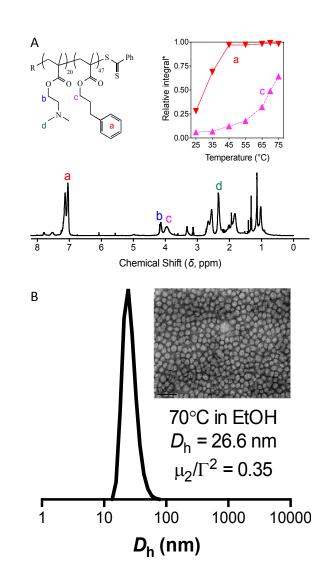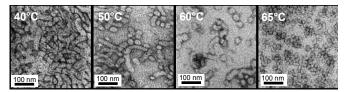
expected integral value (assuming full molecular dissolution) suggesting significantly decreased solvation closer to the backbone.

Figure 6 (A) ^{1}H NMR spectrum of the PDMAEMA$_{20}$-*b*-PPPMA$_{47}$ copolymer at 75°C with an inset plot showing the relative integral values of the side chain aromatic and methoxy hydrogens associated with the core-forming PPPMA block relative to the PDMAEMA solvated coronal chains, and (B) the intensity average size distribution of the PDMAEMA$_{20}$-*b*-PPPMA$_{47}$ copolymer measured in EtOH at 70°C highlighting the presence of nanoaggregates and the TEM image of the same copolymer shown inset for comparative purposes.

These NMR results are consistent with the TEM data indicating that the PDMAEMA$_{20}$-*b*-PPPMA$_{47}$ block copolymer exists at spherical aggregates at 70°C although NMR clearly suggests that at this temperature the aggregates have solvent swollen cores. To further confirm the presence of aggregates at 70°C in EtOH the block copolymer was characterized by DLS at elevated temperature (NB the DLS data in Table 1 was collected at ambient temperature). Figure 6B shows the intensity-average size distribution measured at 70°C, with the

original TEM image shown inset for comparative purposes. DLS clearly demonstrates the presence of aggregates at this higher temperature with a measured D_h of 26.6 nm and corresponding μ_2/Γ^2 of 0.35.

It is these changes in solvation of the core and coronal chains that are responsible for the observed thermoreversible W-S morphology transitions. Enhanced solvation of the nanoaggregate core implies an increasing solvent quality of EtOH for the PPMA core chains. This can, conceptually, result in a lowering of interfacial surface tension and may, alone, be responsible for the observed W-S transition. However, the increase in the degree of core solvation will also change the relative volume fractions of the DMAEMA and PPMA blocks that may change the packing parameter value from that for worms to spheres.[56]

The thermoreversible degelation-gelation phenomenon coupled with the temperature-dependent NMR studies raises another interesting question. While we have demonstrated a clear W-S transition upon heating for the PDMAEMA$_{20}$-b-PPPMA$_{47}$ copolymer, it is not apparent if the transition is step-wise or instantaneous. Additionally, it is not clear whether 70°C represents the critical morphology transition temperature or if the morphology transition occurs at a lower temperature at some critical degree of enhanced core solvation. In an effort to gain some insight into this transitional process the PDMAEMA$_{20}$-b-PPPMA$_{47}$ copolymer was heated to 40, 50, 60 and 65°C, held at each temperature for 5 min., a sample extracted, diluted with EtOH at the same temperature and imaged by TEM, Figure 7.

Figure 7 Representative TEM images of the PDMAEMA$_{20}$-b-PPPMA$_{47}$ block copolymer extracted from EtOH at a concentration of 21 wt% at 40, 50, 60 and 65°C demonstrating the thermally induced W-S morphology transition. 40°C: 100% worms; 50°C: predominantly worms; 60°C: predominantly spheres; 65°C: 100% spheres.

TEM clearly shows that under the experimental conditions employed there is a gradual shift associated with the W-S transition. At 40°C we observe a pure worm phase, while at 50°C we begin to observe a shift towards a spherical morphology although worms represent the major nanoaggregate species. This distribution is switched at 60°C, and at 65°C the transition to a pure sphere phase is complete. These TEM results coincide nicely with the variable temperature ^{1}H NMR data presented above and suggest such facile rearrangement requires some degree of core solvation.

While we have demonstrated degelation-gelation at a concentration of 21 wt% we note that if physical gelation is a result of worm aggregate entanglements then degelation should also be possible by simple dilution below the critical entanglement concentration, giving a second convenient approach for inducing a macroscopic change. Starting with the PDMAEMA$_{20}$-b-PPPMA$_{47}$ copolymer at 21wt% a series of dilutions resulted in degelation at a concentration of 8wt%. Figure 8 shows two digital pictures of this block copolymer at concentrations of 10 and 8wt% demonstrating the macroscopic change.
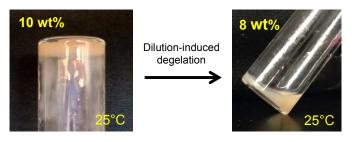

Figure 8 Digital pictures of a 10 wt% gel like state (left) and 8 wt% fluid state (right) in EtOH for the PDMAEMA$_{20}$-b-PPPMA$_{47}$ copolymer highlighting dilution-induced degelation.

Finally, we note that in preliminary observations it appears similar copolymers are able to undergo thermoreversible V-S transitions. For example, Figure 9 shows examples of TEM images for the PDMAEMA$_{20}$-b-PPPMA$_{61}$ copolymer (Table 1 entry 7 whose morphology at room temperature was determined to be vesicular) at 25°C, 70°C and after cooling back to 25°C.
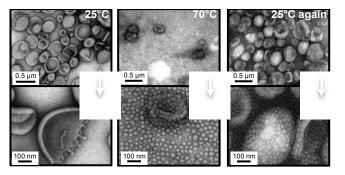

Figure 9 TEM images for the PDMAEMA$_{20}$-b-PPPMA$_{61}$ AB diblock copolymer at 25°C exhibiting a clear vesicular morphology, the same sample after heating to 70°C now existing in a predominantly spherical morphology, and after cooling back to 25°C a mixed S/V phase is observed.

At 25°C the PDMAEMA$_{20}$-b-PPPMA$_{61}$ copolymer exists as vesicles (average D_h = 132.4 nm). Heating to 70°C for 1 h results in a morphology switch to a predominantly spherical phase giving nanoparticles of a reasonably uniform size with D_h's on the order of 20 nm. Cooling the solution back to 25°C over a period of 2-3 days results in a mixture of S + V nanoparticles. These observations further reinforce the notion that thermoreversible morphology transitions may be more common in RAFTDP systems than is currently appreciated. These vesicle-to-sphere transitions are currently being investigated in more detail.

Conclusions

The reversible addition-fragmentation chain transfer dispersion polymerisation (RAFTDP) of 3-phenylpropyl methacrylate (PPMA) with poly[2-(dimethylamino)ethyl methacrylate] (PDMAEMA) macro-CTAs has been examined in EtOH at 70°C. For a fixed total solids content of 21 wt% and average degree of polymerisation ($\overline{X}_n$) of the stabilising PDMAEMA macro-CTA of 20 we observe the full spectrum of nanoparticle morphologies (spheres, worms and vesicles) with increasing $\overline{X}_n$ of PPMA, which highlights the suitability of PPMA as a comonomer in RAFTDP. Replacing the PDMAEMA$_{20}$ macro-CTA with a PDMAEMA$_{35}$ species also facilitated the facile access to the full range of morphologies although phases tended to be noticeably more mixed. Interestingly however, we observed differing morphological phases for PDMAEMA$_{20}$-PPPMA$_y$ and PDMAEMA$_{35}$-PPPMA$_y$ of similar overall block ratios highlighting how self-assembly is complex and dependent on both the solvophilic and solvophobic block lengths. In addition to varying $\overline{X}_n$ for the PPMA block we also highlighted how morphology can be tuned by a systematic variation in the total solids content for a fixed block copolymer composition with distinct sphere, worm and mixed sphere/worm phases being accessible simply by varying concentration. In the case of the PDMAEMA$_{20}$-b-PPPMA$_{47}$ copolymer interesting thermoreversible macroscopic degelation-gelation was observed that was accompanied by a fundamental worm-to-sphere morphological transition. This system was characterised via variable temperature ^{1}H NMR spectroscopy and dynamic light scattering. ^{1}H NMR studies indicated that the rapid and facile morphology transition was facilitated by a significant increase in solvation of the nanoaggregate core blocks that also significantly increased their chain mobility. The precise physical reason for the morphology transition is unclear but may be due to a change in the interfacial surface energy with increasing temperature and or be associated with a change in the volume fractions of the coronal and core blocks with increasing core solvation. We also demonstrated that macroscopic degelation of the worm nanoaggregates can be affected by simple dilution below some critical entanglement concentration. Finally, in preliminary experiments we have shown that thermoreversible vesicle-to-sphere transitions may are also possible with similar DMAEMA-PPMA based block copolymers although appear to be kinetically slower than the reversible worm-to-sphere changes.

Acknowledgements

Notes and references

School of Chemical Engineering, Centre for Advanced Macromolecular Design, UNSW Australia, University of New South Wales, Kensington, Sydney, 2052 NSW, Australia.

1. Y. Mai and A. Eisenberg, *Chem. Soc. Rev.*, 2012, **41**, 5969-5985.
2. G. Riess, *Prog. Polym. Sci.*, 2003, **28**, 1107-1170.
3. J. Rodríguez-Hernández, F. Chécot, Y. Gnanou and S. Lecommandoux, *Prog. Polym. Sci.*, 2005, **30**, 691-724.
4. S. C. Owen, D. P. Y. Chan and M. S. Shoichet, *Nano Today*, 2012, **7**, 53-65.
5. M. Moffitt, K. Khougaz and A. Eisenberg, *Acc. Chem. Res.*, 1996, **29**, 95-102.
6. Y. Mai and A. Eisenberg, *Acc. Chem. Res.*, 2012, **45**, 1657-1666.
7. L. Jia, D. Lévy, D. Durand, M. Impéror-Clerc, A. Cao and M.-H. Li, *Soft Matter*, 2011, **7**, 7395-7403.
8. I. LaRue, M. Adam, E. B. Zhulina, M. Rubinstein, M. Pitsikalis, N. Hadjichristidis, D. A. Ivanov, R. I. Gearba, D. V. Anokhin and S. S. Sheiko, *Macromolecules*, 2008, **41**, 6555-6563.
9. Y. Yu and A. Eisenberg, *J. Am. Chem. Soc.*, 1997, **119**, 8383-8384.
10. R. Nagarajan, in *Solvents and Self-Organization of Polymers*, eds. S. E. Webber, P. Munk and Z. Tuzar, Kluwer Academic, 1996, vol. 327, pp. 121-166.
11. S. Abbas, Z. Li, H. Hassan and T. P. Lodge, *Macromolecules*, 2007, **40**, 4048-4052.
12. I. LaRue, M. Adam, M. Pitsikalis, N. Hadjichristidis, M. Rubinstein and S. S. Sheiko, *Macromolecules*, 2006, **39**, 309-314.
13. J. Jennings, M. Beija, A. P. Richez, S. D. Cooper, P. E. Mignot, K. J. Thurecht, K. S. Jack and S. M. Howdle, *J. Am. Chem. Soc.*, 2012, **134**, 4772-4781.
14. G. Liu, Q. Qiu and Z. An, *Polym. Chem.*, 2012, **3**, 504-513.
15. D. Zehm, L. P. D. Ratcliffe and S. P. Armes, *Macromolecules*, 2013, **46**, 128-139.
16. S. Sugihara, A. Blanazs, S. P. Armes, A. J. Ryan and A. L. Lewis, *J. Am. Chem. Soc.*, 2011, **133**, 15707-15713.
17. M. Semsarilar, V. Ladmiral, A. Blanazs and S. P. Armes, *Langmuir*, 2013, **29**, 7416-7424.
18. M. Semsarilar, V. Ladmiral, A. Blanazs and S. P. Armes, *Langmuir*, 2012, **28**, 914-922.
19. A. Blanazs, A. J. Ryan and S. P. Armes, *Macromolecules*, 2012, **45**, 5099-5107.
20. P. Chambon, A. Blanazs, G. Battaglia and S. P. Armes, *Macromolecules*, 2012, **45**, 5081-5090.
21. B. Charleux, G. Delaittre, J. Rieger and F. D'Agosto, *Macromolecules*, 2012, **45**, 6753-6765.
22. L. Houillot, C. Bui, C. Farcet, C. Moire, J. A. Raust, H. Pasch, M. Save and B. Charleux, *ACS Appl. Mater. Interfaces*, 2010, **2**, 434-442.
23. S. Kessel, N. P. Truong, Z. Jia and M. J. Monteiro, *J. Polym. Sci., Part A: Polym. Chem.*, 2012, **50**, 4879-4887.
24. W. M. Wan, X. L. Sun and C. Y. Pan, *Macromol. Rapid Commun.*, 2010, **31**, 399-404.
25. W.-M. Wan and C.-Y. Pan, *Polym. Chem.*, 2010, **1**, 1475-1484.
26. J.-T. Sun, C.-Y. Hong and C.-Y. Pan, *Polym. Chem.*, 2013, **4**, 873-881.
27. C. Q. Huang, Y. Wang, C. Y. Hong and C. Y. Pan, *Macromol. Rapid Commun.*, 2011, **32**, 1174-1179.
28. C.-Q. Huang and C.-Y. Pan, *Polymer*, 2010, **51**, 5115-5121.
29. W.-D. He, X.-L. Sun, W.-M. Wan and C.-Y. Pan, *Macromolecules*, 2011, **44**, 3358-3365.
30. M. Semsarilar, V. Ladmiral, A. Blanazs and S. P. Armes, *Polym. Chem.*, 2014, **5**, DOI: 10.1039/c1034py00201f.
31. W.-M. Wan and C.-Y. Pan, *Macromolecules*, 2010, **43**, 2672-2675.
32. L. P. D. Ratcliffe, A. Blanazs, C. N. Williams, S. L. Brown and S. P. Armes, *Polym. Chem.*, 2014, **5**, DOI: 10.1039/c1034py00203b.

33. L. A. Fielding, M. J. Derry, V. Ladmiral, J. Rosselgong, A. M. Rodrigues, L. P. D. Ratcliffe, S. Sugihara and S. P. Armes, *Chem. Sci.*, 2013, **4**, 2081-2087.
34. Y. Li and S. P. Armes, *Angew. Chem. Int. Ed.* , 2010, **49**, 4042-4046.
35. M. Semsarilar, E. R. Jones, A. Blanazs and S. P. Armes, *Adv Mater*, 2012, **24**, 3378-3382.
36. S. Sugihara, S. P. Armes, A. Blanazs and A. L. Lewis, *Soft Matter*, 2011, **7**, 10787-10793.
37. Z. An, Q. Shi, W. Tang, C.-K. Tsung, C. J. Hawker and G. D. Stucky, *J. Am. Chem. Soc.*, 2007, **129**, 14493-14499.
38. J. Rieger, C. Grazon, B. Charleux, D. Alaimo and C. Jérôme, *J. Polym. Sci., Part A: Polym. Chem.*, 2009, **47**, 2373-2390.
39. Y. Pei and A. B. Lowe, *Polym. Chem.*, 2014, **5**, 2342-2351.
40. S. H. Thang, Y. K. Chong, R. T. A. Mayadunne, G. Moad and E. ERizzardo, *Tetrahedron Letts.*, 1999, **40**, 2435-2438.
41. C. A. Dreiss, *Soft Matter*, 2007, **3**, 956-970.
42. S. R. Raghaven and J. F. Douglas, *Soft Matter*, 2012, **8**, 8539-8546.
43. V. Ladmiral, M. Semsarilar, I. Canton and S. P. Armes, *J. Am. Chem. Soc.*, 2013, **135**, 13574-13581.
44. R. Verber, A. Blanazs and S. P. Armes, *Soft Matter*, 2012, **8**, 9915-9922.
45. A. Blanazs, R. Verber, O. O. Mykhaylyk, A. J. Ryan, J. Z. Heath, C. W. Douglas and S. P. Armes, *J. Am. Chem. Soc.*, 2012, **134**, 9741-9748.
46. J. van Stam, S. Creutz, F. C. De Schryver and R. Jérôme, *Macromolecules*, 2000, **3**, 6388-6395.
47. T. Nicolai, O. Colombani and C. Chassenieux, *Soft Matter*, 2010, **6**, 3111-3118.
48. P. Claudy, J. M. Létoffé, Y. Camberlain and J. P. Pascault, *Polym. Bull.*, 1983, **9**, 208-215.
49. K. Ute, N. Miyatake and K. Hatada, *Polymer*, 1995, **36**, 1415-1419.
50. M. Štěpánek, K. Podhájecká, E. Tesařová, K. Procházka, Z. Tuzar and W. Brown, *Langmuir*, 2001, **17**, 4240-4244.
51. M. Tian, A. Qin, C. Ramireddy, S. E. Webber, P. Munk, Z. Tuzar and K. Procházka, *Langmuir*, 1993, **9**, 1741-1748.
52. J. van Stam, S. Creutz, F. C. De Schryver and R. Jérôme, *Macromolecules*, 2000, **33**, 6388-6395.
53. H. Lee, G. Tae and Y. H. Kim, *Macromol. Res.*, 2008, **16**, 614-619.
54. G. Sakellariou, A. Siakali-Kioulafa and N. Hadjichristidis, *Int. J. Polym. Anal. Ch.*, 2003, **8**, 269-277.
55. T. K. Mandal and E. M. Woo, *Macromol. Chem. Phys.*, 1999, **200**, 1143-1149.
56. H. Huang, R. Hoogenboom, M. A. M. Leenen, P. Guillet, A. M. Jonas, U. S. Schubert and J.-F. Gohy, *J. Am. Chem. Soc.*, 2006, **128**, 3784-3788.